JOURNAL OF CATALYSIS 108, 304–322 (1987)

An Integrated Study of $Pt/WO_3/SiO_2$ Catalysts for the NO–CO Reaction

II. TEM Investigation of Overlayer Formation on Model $Pt–WO_3/SiO_2$ Catalysts

J. R. REGALBUTO,[1] C. W. ALLEN,*[,2] AND E. E. WOLF†[,3]

*Departments of †Chemical Engineering and *Metallurgical Engineering and Material Science, University of Notre Dame, Notre Dame, Indiana 46556*

Received November 6, 1986; revised June 22, 1987

Model $Pt/WO_3/SiO_2$ catalysts, prepared by "impregnation" of a silica-covered TEM grid using the same precursor salts and pretreatment steps as those used for supported catalysts, were characterized with TEM by analyzing the same catalyst regions through the series of pretreatment steps. Overlayers appeared after a second calcination step following Pt impregnation. By a series of control experiments the overlayers were shown not to arise from carbon contamination, from impurities in the silica or Pt precursor, or from aging under ambient conditions. On the other hand, the mobility of WO_3 was indicated. These observations qualitatively correlate to previous characterization of the real catalysts and suggest that the SMSI state in $Pt/WO_3/SiO_2$ catalysts arises from mobile, monodisperse species of WO_3 formed during the second, low-temperature calcination step.

INTRODUCTION

The morphology of the $Pt/WO_3/SiO_2$ catalysts is quite complex. In part I of this series of papers (*1*) on these catalysts, CO chemisorption, X-ray diffraction (XRD), and X-ray photoelectron spectroscopy (XPS) were used to characterize the catalyst's morphology. The results of the said studies indicated that chemisorption suppression occurred without the corresponding changes in crystallite size as indicated by XRD. Furthermore, associated with this, changes in the oxidation state of the catalysts were detected by XPS. These results were explained via a decoration model similar to that postulated for Pt/TiO_2 catalysts, as presented recently in a review paper on the subject (*2*). While postulated for a new catalyst system ($Pt/WO_3/SiO_2$), the model is similar to others proposed for more common SMSI catalysts (*2*). For example, the SMSI state in TiO_2 catalysts is produced by a high-temperature (500°C) reduction of the catalyst without an intermediate calcination step. Decoration is thought to occur as partially reduced moieties of the support, TiO_x ($x < 2$), migrate onto the metal surface.

While ample support for this type of morphological model has come from Auger electron spectroscopy, XPS, and infrared and chemisorption studies (*2*), direct detection of decorating species by electron microscopy has been difficult to obtain. No evidence for a decoration model has been obtained in a number of studies of both real (three-dimensional) and model (two-dimensional) Pt/TiO_2 (*3–6*) and Rh/TiO_2 (*7*) catalysts. In these, the characteristic features of the SMSI state were first associated with the formation of metal crystallites which assumed a hexagonal, flat "pillbox" morphology. It was also reported that TiO_2 was reduced to Ti_4O_7 in the SMSI state (*4*, *5*),

[1] Present address: Department of Chemical Engineering, University of Illinois at Chicago, Box 4348, Chicago, IL 60680.

[2] Present address: EM Center for Materials Research, Argonne National Laboratory, Argonne, IL 60439.

[3] To whom correspondence should be addressed.

0021-9517/87 $3.00

and it was suggested that thin Pt crystallites formed a structural relationship with the Ti_4O_7. Suppression of chemisorption was explained by the hypothesis that this relationship might require the formation of chemical bonds between Pt and the support.

Overlayer structures have finally been detected in studies of real Rh/TiO_2 (*8*) and model Ni/TiO_2 (*9*) catalysts. In these studies, however, a reduction temperature 220–300°C higher than normal was required to produce them unless TiO_2 was purposefully placed over the metal (*8*).

To investigate the SMSI morphology of $Pt/WO_3/SiO_2$ catalysts, a technique was chosen such that the characterization of the real catalysts (*1*) would be paralleled in the TEM studies of model catalysts. Planar silica substrates were used as the catalyst support to facilitate the analysis of micrographs. WO_3 and Pt were deposited on them by "impregnation"; that is, the same precursor solutions of ammonium tungstate and chloroplatinic acid as had been used for the real catalysts were carefully spread over the SiO_2 substrate and allowed to evaporate. Model Pt/C and Ir/C have been prepared in a similar manner (*10, 11*) wherein carbon flakes were sprayed with solutions of chloroplatinic or chloroiridic acid. These samples were reduced before they were mounted on microscope grids. In this work the WO_3 and Pt presursors were placed directly onto a microscope grid, and all steps of the model catalyst pretreatment were studied, thus representing a new variant of studies of the effect of gas treatments on model catalysts (*12*). For comparison, several micrographs of the real $Pt/WO_3/SiO_2$ catalysts are included.

A key difference in the SMSI state of $Pt/WO_3/SiO_2$ and also Pd/La_2O_3 (*13*) and $Pd/La_2O_3/SiO_2$ (*14*) catalysts, and that of TiO_2-supported catalysts, is that a calcination step is used in the preparation of the former catalysts. Because each step of catalyst preparation was studied, the role of the calcination step in the genesis of the SMSI state in $Pt/WO_3/SiO_2$ model catalysts was demonstrated. The results from TEM characterization concur with the previous characterization studies presented in part I (*1*) of this series, as well as with the NO–CO reaction kinetic results to follow in part III (*15*).

EXPERIMENTAL

Apparatus

A JEOL JEM 100C scanning transmission electron microscope (STEM) was used for most of the microscopy. Some of the work on model catalysts was performed with a Phillips 400T microscope at Arizona State University's Department of Physics. A high-resolution objective lens pole piece, a side entry goniometer, and a tungsten filament were used with the JEOL instrument; the standard pole piece and side entry goniometer, and a LaB_6 filament, were used with the Phillips microscope. Both were operated at 120 kV accelerating potential.

Most imaging was done in the bright field mode using an objective aperture to enhance diffraction contrast. Electron diffraction patterns from sufficiently large sample areas contained Debye–Scherrer rings which were used for the determination of bulk crystalline phases. Individual crystallites were identified in the following manner. First, the sample orientation was tilted until the crystallite was in the proper orientation to Bragg diffract. The diffraction pattern was then searched for that spot which illuminated the crystallite in the dark field mode, i.e., the spot due to diffraction from the crystallite. Once found, the spot could be easily associated to a particular crystalline phase.

Procedures

The model catalyst supports consisted of 200-mesh gold microscope grids (Ladd Research Ind.) covered with a planar silica substrate. The use of gold grids and the removal of the silica substrate organic

backing were necessary to keep the grids inert during the calcination and reduction steps. The active components were deposited on the grids by carefully spreading a small drop of a solution containing the catalyst precursor salts (ammonium tungstate, chloroplatinic acid). This method was devised to mimic the impregnation procedures used in the preparation of the real catalysts.

After deposition of the catalyst precursor salts, the microscope grids were placed in a quartz flow reactor where they were subjected to pretreatments similar to those for the real catalysts. After a given pretreatment step, the grids were transferred to the microscope sample holder, which required atmospheric exposure. (The real catalysts had also been exposed to the atmosphere between pretreatments.) the following pretreatment steps were used:

1. impregnation with ammonium metatungstate
2. vacuum dry, 80°C, 2 h
3. calcination, 700°C, 3 h, in air
4. reimpregnation with chloroplatinic acid
5. vacuum dry, 80°C, 2 h
6. calcination, 300°C, 3 h, in air
7. reduction, 400°C, 3 h, in H_2.

The calcination performed after the tungsta impregation step will be referred to hereafter as the "high-temperature" or "first" calcination, while that after the Pt impregnation will be referred to as the "low-temperature" or "second" calcination.

Distributions of WO_3 and Pt on the SiO_2 substrates were not uniform. In several samples much of the WO_3 deposited in sheets, with smaller tungsta crystallites appearing at the sheet edges. Platinum deposited in aggregates of very fine particles. Regions which contained the smaller WO_3 crystallites in close proximity to Pt clumps were chosen as those most representative of the real catalysts.

A total of five model samples were prepared over the course of this investigation: two each of $Pt/WO_3/SiO_2$ and Pt/SiO_2, and one of WO_3/SiO_2. The same behavior was observed on duplicate samples. Pt/SiO_2 and WO_3/SiO_2 samples were used to evaluate the behavior of each catalyst component separately.

Photographs were normally taken within hours after the completion of the pretreatments. After one pretreatment (the second calcination of the $Pt/WO_3/SiO_2$ catalysts), however, the catalysts were stored in air at room temperature for 6 weeks. A control experiment was performed to ensure that results were not affected by this aging period. Additionally, similar results were obtained over a second $Pt/WO_3/SiO_2$ catalyst which had been aged for a shorter period.

RESULTS

High-Temperature Calcination Step

Two micrographs of the same area of catalyst which illustrate the impregnation and high-temperature calcination of WO_3 are shown in Fig. 1. After the impregnation and drying step, Fig. 1a, the precursor salt did not Bragg diffract; that is, it was not appreciably crystalline at this stage. Considerable migration occurred during the 700°C calcination as WO_3 crystallites were formed. A diffraction pattern from a typical region of the catalyst at this step is shown in Fig. 4a. The large crystalline needle, marked (B) in Fig. 1b, apparently formed from the corresponding wedge-shaped section of the amorphous precursor (A).

Pt Impregnation and Drying Step

After the tungsta crystals were formed, the sample was reimpregnated with chloroplatinic acid and dried under vacuum. Subsequent treatments were the second calcination and the reduction. Figures 2 and 3 consist of two series of micrographs each showing a different area of catalyst after (a) drying, (b) calcination, and (c) reduction, respectively. In Figs. 2a and 3a the larger and smoother WO_3 crystallites are easily

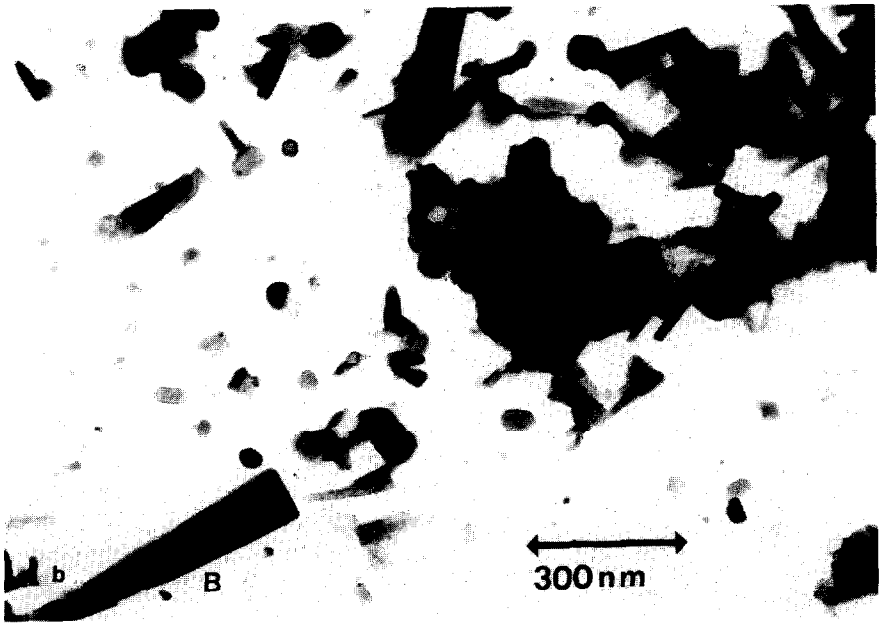

FIG. 1. Formation of WO_3 (a) after impregnation and drying, (b) after first high-temperature calcination.

distinguishable from aggregates of the Pt precursor. WO_3 crystallites could also be identified crystallographically. The Pt precursor after the drying stage did not produce Debye rings.

Pt Calcination Step

After calcination, Figs. 2b and 3b, thin films or overlayers appeared on many WO_3 and Pt crystallites. These are indicated by arrows marked "1." The overlayers, between 30 and 40 Å wide, appeared amorphous as they were not observed to Bragg diffract as the sample orientation was tilted ±40°. Comparing the same area at the dried and calcined stages, many tungsta crystallites (labeled "2"), which had sharp edges and exhibited high contrast at the drying step, appeared to lose their definition of shape and decrease in contrast after the calcination. In other words, these small WO_3 crystallites appeared to spread at this step. Upon calcination the Pt crystallites displayed less graininess than observed previously, and so appeared to sinter. An electron diffraction pattern of a typical section taken at this stage (Fig. 4b) revealed diffuse Pt rings in addition to the WO_3 pattern.

The appearance of overlayers was not observed in all areas, however. Of seven areas photographed through the pretreatment process, overlayers were clearly observed in three.

Pt Reduction Step

Upon reduction the same chromatic effect that had been observed for the real catalysts (they turned black) was observed (optically) in heavily loaded regions of the model catalyst. Crystallites of WO_3 appeared to change little in structure. Electron diffraction (Fig. 4c) revealed that like the real catalysts, hydrogen tungsten bronzes (HTB) had formed. (Only very minor structural changes accompany the formation of HTB, as hydrogen protons are incorporated into the oxide lattice (*16, 17*)). The clearest difference in the diffraction patterns of fully oxidized WO_3 and HTB was the disappearance of the WO_3 (111) ring, a change also noted in X-ray diffraction studies of the real catalysts (*1*). Analysis of smaller *d*-spacings in the diffraction pattern of the reduced form revealed that the pattern could not be attributed to one individual HTB. A solid solution of $H_{0.1}WO_3$, $H_{0.33}WO_3$, and/or $H_{0.5}WO_3$ likely formed.

In the reduced catalysts, Pt crystallites sintered further. The overlayers were slightly smoother in shape and some sections broadened somewhat. Sections which broadened noticeably are labeled "3" in Figs. 2b and 3b and "3′" in Figs. 2c and 3c.

Overlayers were not stable to sustained electron beam exposure. Pictured in Fig. 5a is a very broad (80–90 Å) overlayer surrounding a large HTB crystallite (A). Wide overlayers were also seen on the surrounding Pt crystallites (B). After only 4 min of beam exposure, the overlayer had virtually disappeared from the HTB. While they had thinned, overlayers were still present surrounding Pt, Fig. 5b. The same behavior was observed in many other regions. However, in some cases stable overlayers were observed on HTB crystallites which appeared to be in very good contact with a Pt crystallite. These areas underwent approximately 15 min of beam exposure without showing any overlayer degradation.

Model WO_3 and Pt Single-Component Catalysts

Model Pt–SiO_2. Seven separate regions of a sample containing only Pt on SiO_2 were examined before and after calcination, and again after 10 weeks storage in air. The behavior of the area shown in Fig. 6 is representative of that observed in the other areas. After the drying step, Fig. 6a, Pt once again appeared in grainy clumps of very small particles and exhibited no crystallinity. After calcination (Fig. 6b), Pt

crystallites grew slightly in size. However, overlayers were not observed in any of the regions examined. Furthermore, after 10 weeks storage under ambient conditions, virtually no changes were observed.

Model WO_3–SiO_2. Several regions of a WO_3–SiO_2 sample were photographed first after a 700°C reduction, and again after a 300°C calcination. Many of the areas displayed no appreciable change after the second calcination. Representative micrographs of one area in which changes were observed are shown in Fig. 7. After the 700°C calcination (Fig. 7a), the two crystallites (A) and (B) had generally smooth surfaces and well-defined edges. Figure 7b, taken after the second calcination, was at a slightly different orientation than Fig. 7a. This may be part of the reason for the change in appearance of crystallite (B). Crystallite (A) clearly became facetted, and displayed regions (arrowed) in which overlayers appeared to form.

Real Pt/WO_3–SiO_2 Catalyst

In Fig. 8 a typical region of a reduced 3.8 wt% Pt/25 wt% WO_3–SiO_2 catalyst is shown. It is quickly apparent that the porous real catalyst is much more complex than the planar model catalysts. Based on visual differences between this figure and a real catalyst containing only WO_3/SiO_2, Pt crystallites appeared to form as the smaller, often straight-sided crystallites ("1"). The larger, irregularly shaped patches correspond to HTBs ("2"). Spotty HTB and Pt rings appeared in the diffraction pattern from this region. Several structures which could possibly be interpreted as overlayers did appear, but due to the complexity of the sample and insufficient resolution any such assignment would be speculative.

DISCUSSION

The results of this TEM investigation of the preparation steps of model $Pt/WO_3/SiO_2$

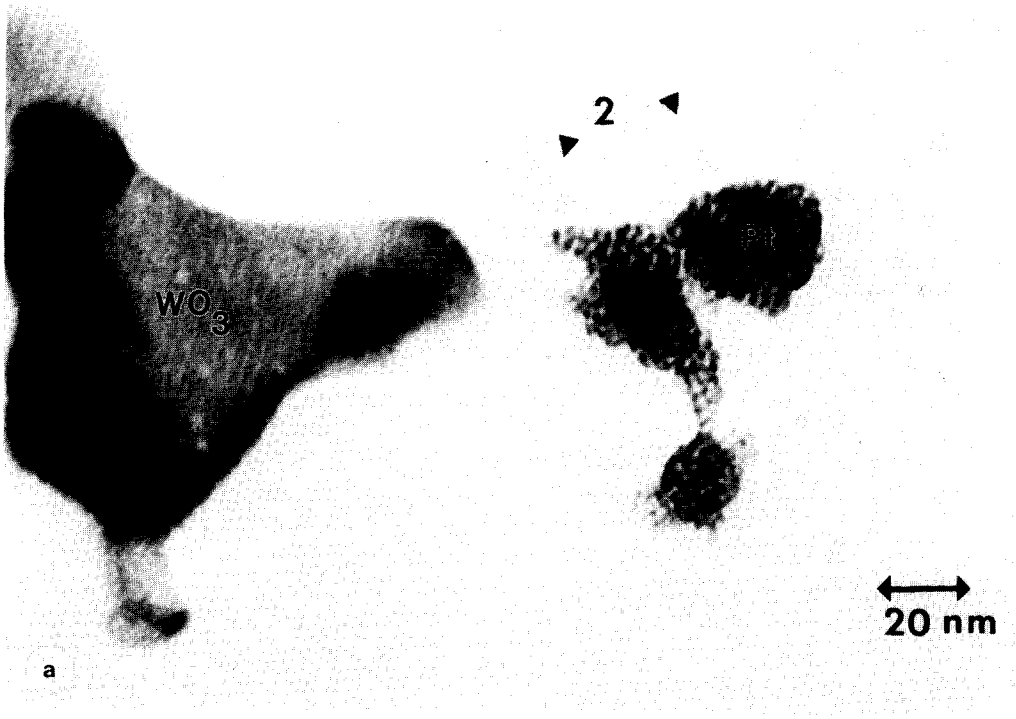

FIG. 2. Pt–WO_3 model catalyst (a) after Pt impregnation and drying, (b) after second low-temperature calcination, and (c) after reduction.

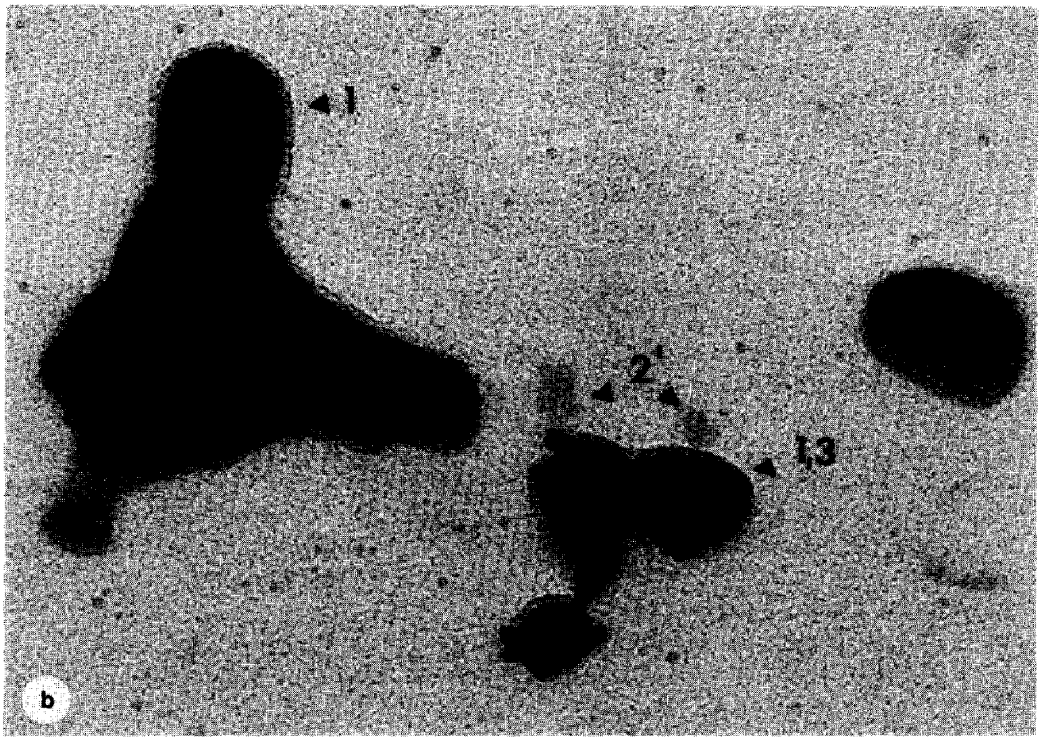

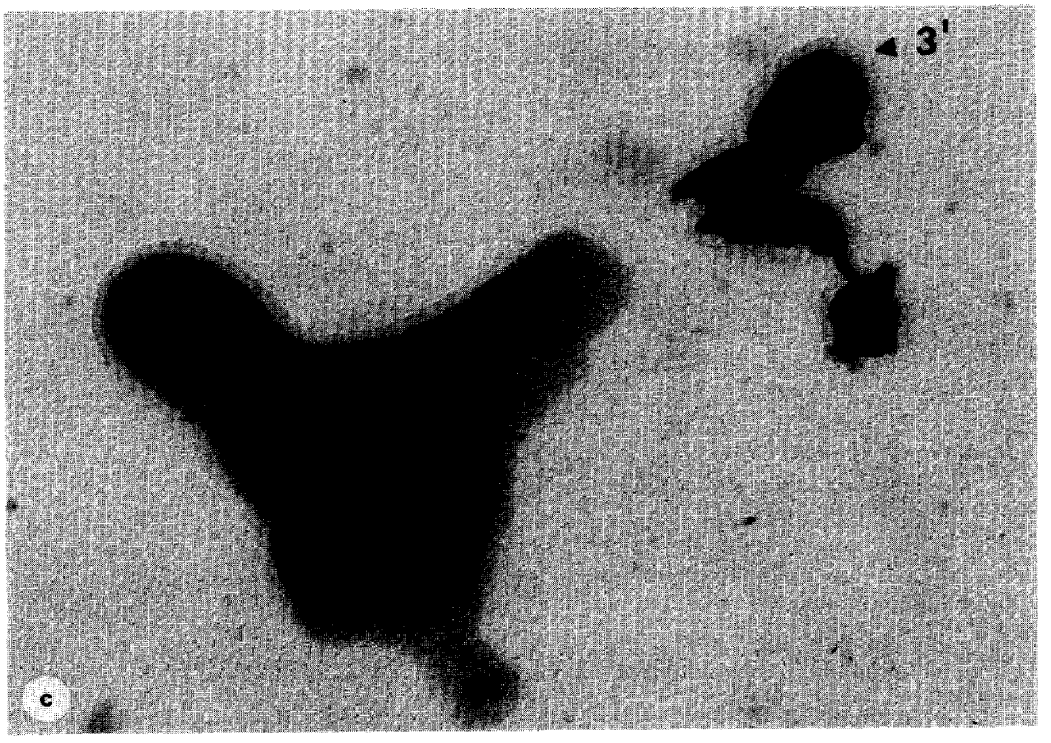

FIG. 2—*Continued.*

catalysts, which paralleled the preparation of the real catalysts, can be summarized as follows:

(1) High-temperature calcination: WO_3 crystallites formed from the previously amorphous precursor salt

(2) Pt impregnation and drying: no change in WO_3 crystallites, appearance of Pt in grainy, noncrystalline aggregates

(3) Second calcination: some WO_3 crystallites appeared to lose material, Pt crystallites sintered slightly, and amorphous overlayers appeared on many Pt and WO_3 crystallites

(4) Reduction: no significant change in WO_3 crystallite shapes but a conversion to HTBs, Pt crystallites agglomerated further, overlayers spread slightly, characteristic black color observed

(5) Upon exposure to the electron beam, overlayers disappeared almost completely from WO_3 crystallites not in close contact with Pt, but did not disappear altogether from Pt crystallites.

In viewing WO_3/SiO_2 and Pt/SiO_2 single-component model catalysts it was found that:

(6) No overlayers were formed on Pt after calcination

(7) Smooth, well-defined WO_3 crystallites were present after a high-temperature calcination. Some of these became facetted and appeared to form overlayers during the second calcination.

Studies of real $Pt/WO_3/SiO_2$ catalysts revealed:

(8) fairly uniformly dispersed patches of bulk WO_3 and

(9) smaller, often regularly shaped Pt crystallites in close proximity to WO_3 patches.

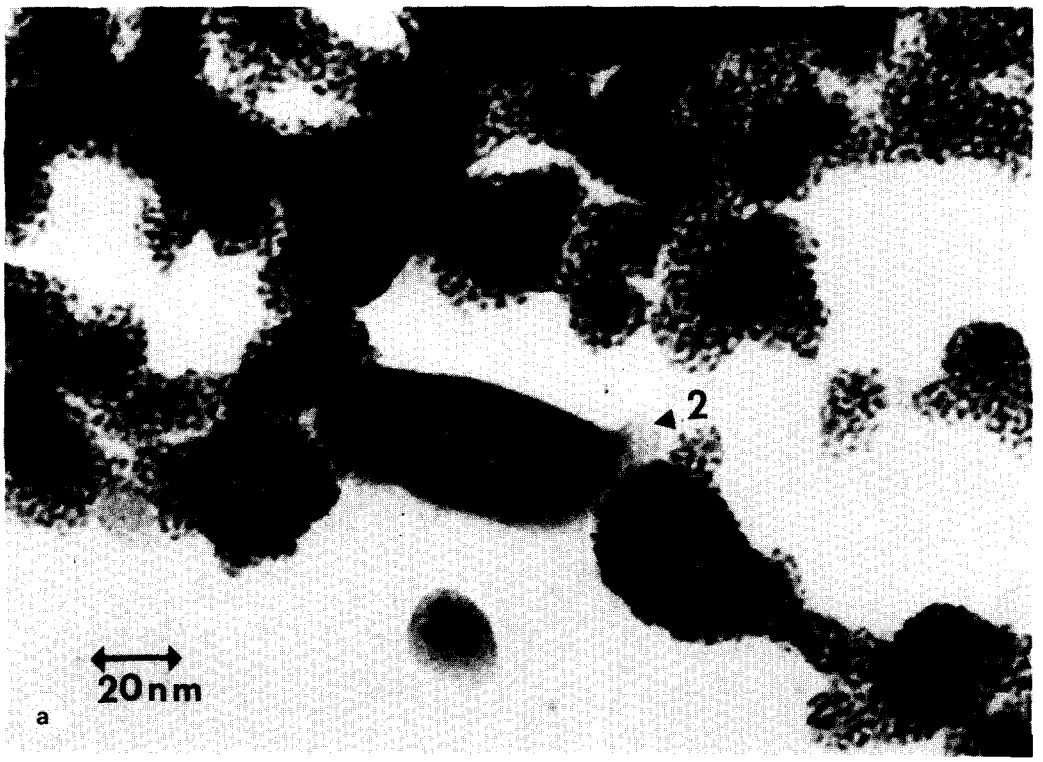

FIG. 3. Pt–WO_3 model catalyst (a) after Pt impregnation and drying, (b) after second low-temperature calcination, and (c) after reduction.

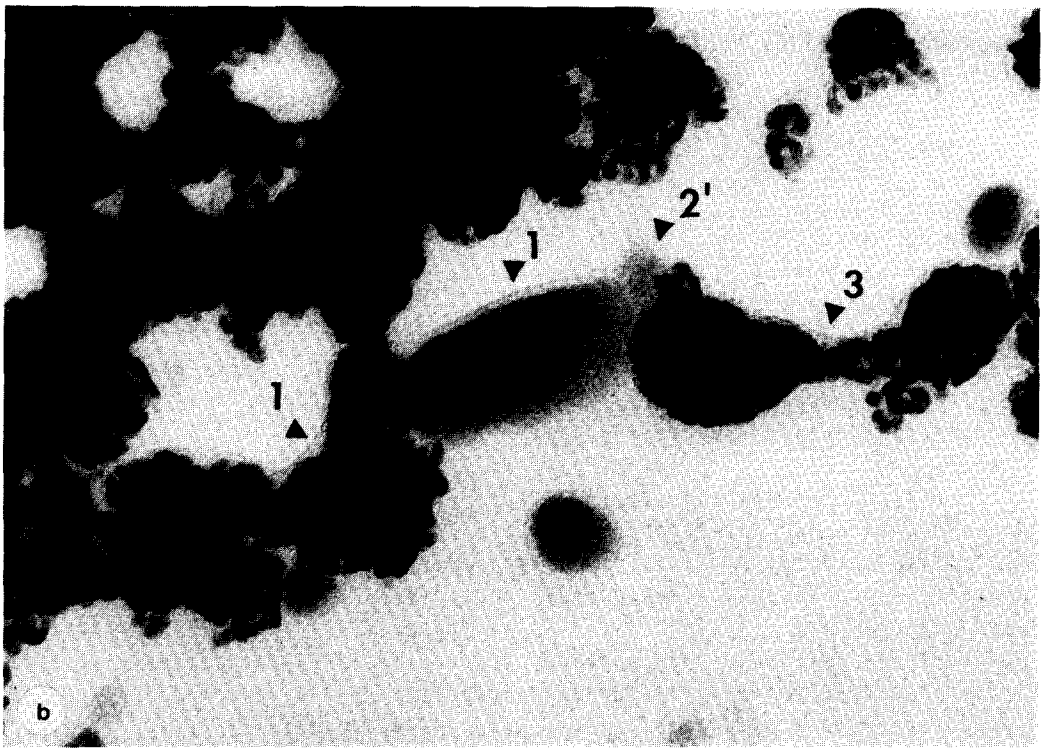

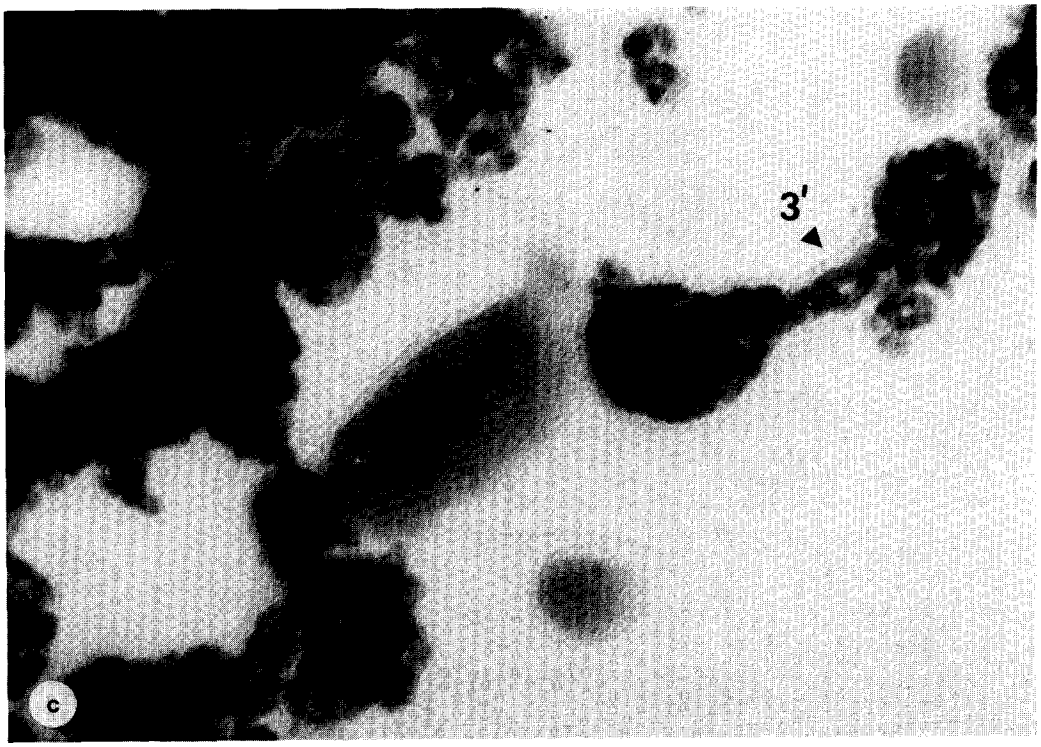

FIG. 3—*Continued.*

The importance of the preparation procedure on the eventual morphology of the model catalyst crystallites becomes evident in the present study. The impregnation and drying step determined to a large extent the final morphology of Pt. The second calcination step was significant in that it led to the appearance of overlayers on some of the WO_3 crystallites, and on some Pt crystallites in close proximity. Overlayers were not found in all regions but in three out of seven analyzed. Calcination caused sintering of the Pt crystallites but did not induce other significant morphological changes. Reduction changed the oxidation state of WO_3 to HTB, and presumably to WO_2, and resulted in further spreading of the overlayers.

One of the questions that must be addressed concerns the chemical nature of the overlayers. Direct positive identification was not possible at the resolution that this work was conducted. The overlayers did not diffract at any particular orientation so they could not be identified crystallographically. As the overlayers were unstable under the wide electron beam employed (about 2000 Å), they would disintegrate even faster under the more intense beam required for EDAX analysis. Furthermore, EDAX would not have sufficient spatial resolution for positive identification of such thin features in close proximity to Pt crystallites. Therefore identification can be made only indirectly by discounting processes which could account for the formation of overlayers, and by inference with the previous characterization of the real supported catalysts.

First, overlayers could arise from carbon contamination due to electron beam irradiation of carbon containing impurities pres-

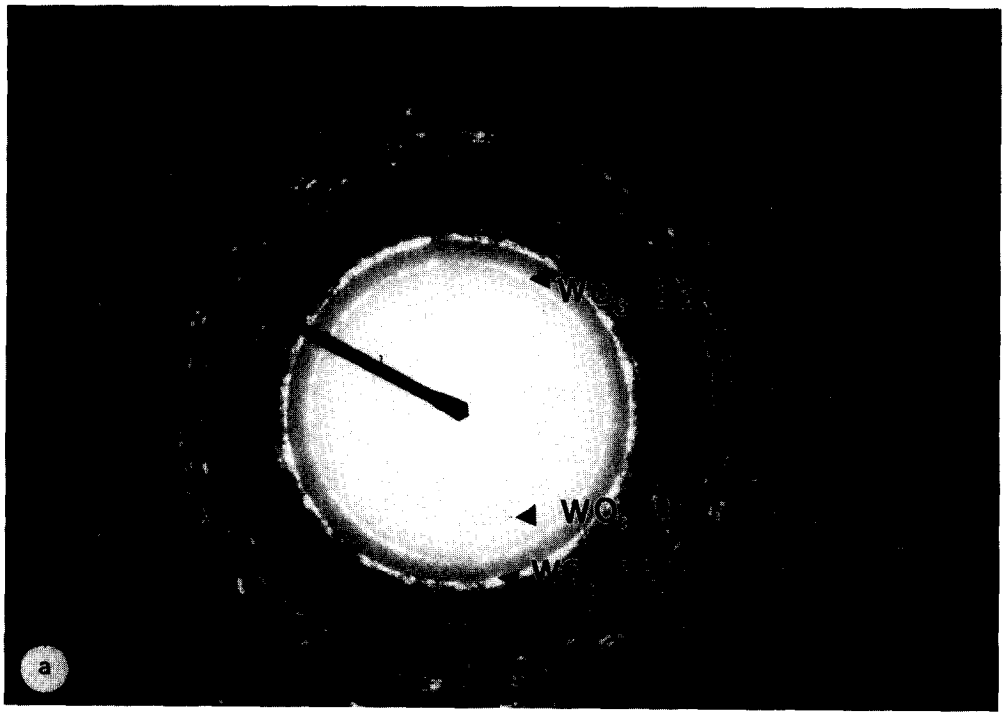

FIG. 4. Electron diffraction patterns of the model catalyst during different stages of preparation, (a) after first high-temperature calcination, (b) area containing high Pt concentration after low-temperature calcination, (c) area containing WO_3 in the form of HTB after reduction. A camera length of 120 cm was used for all diffraction patterns.

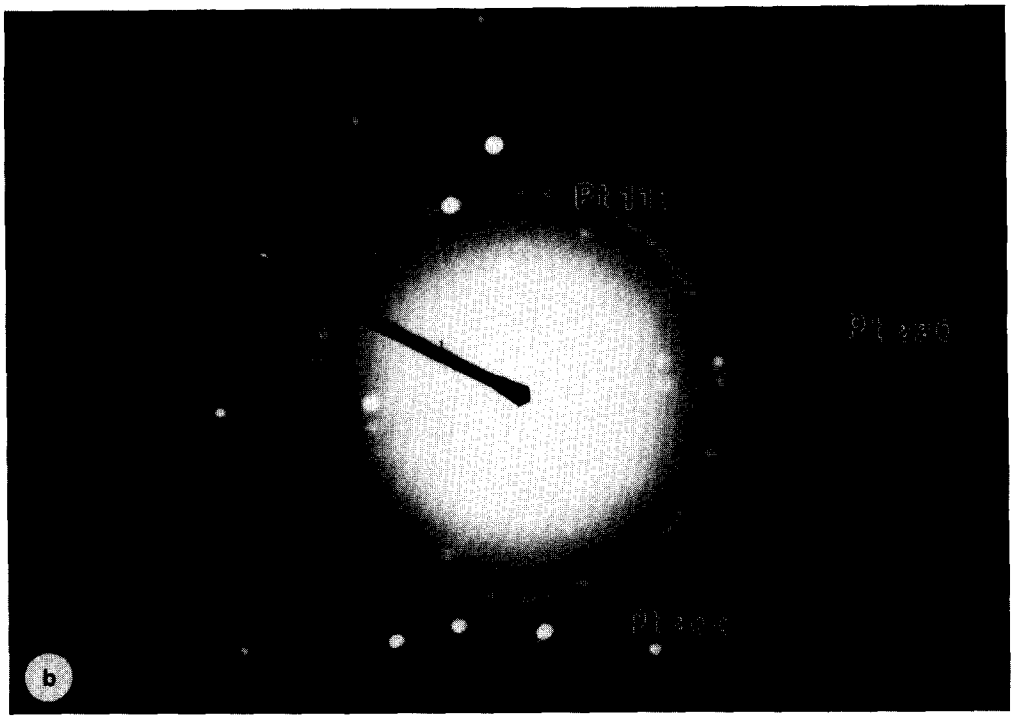

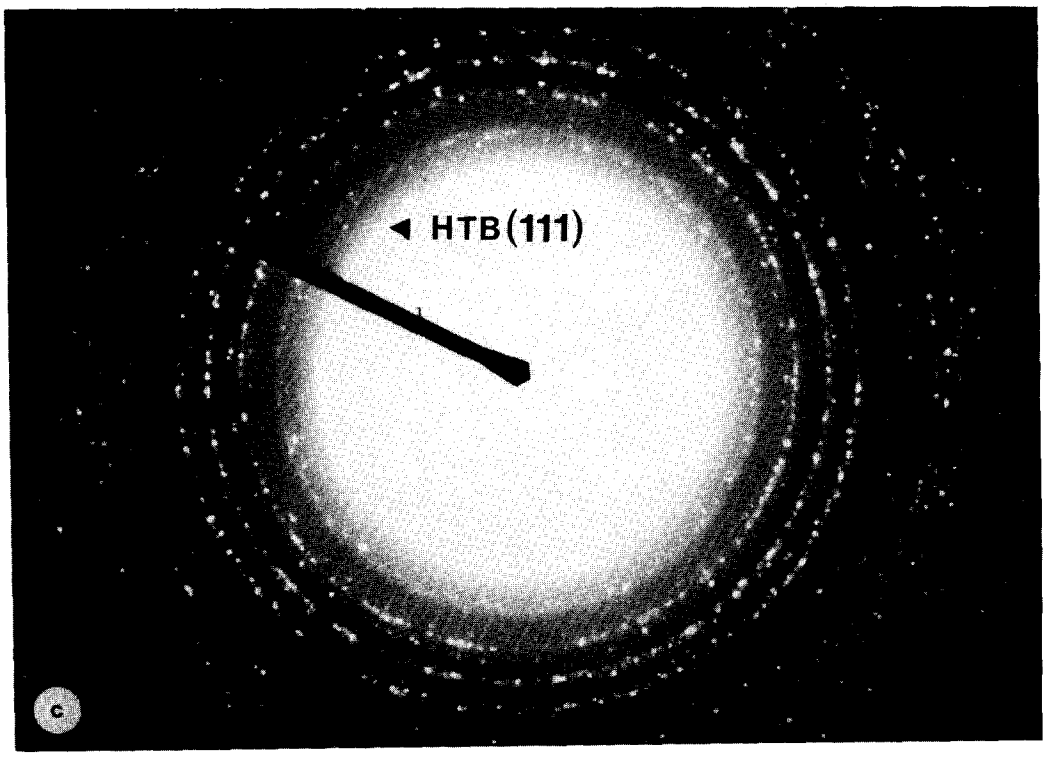

FIG. 4—*Continued.*

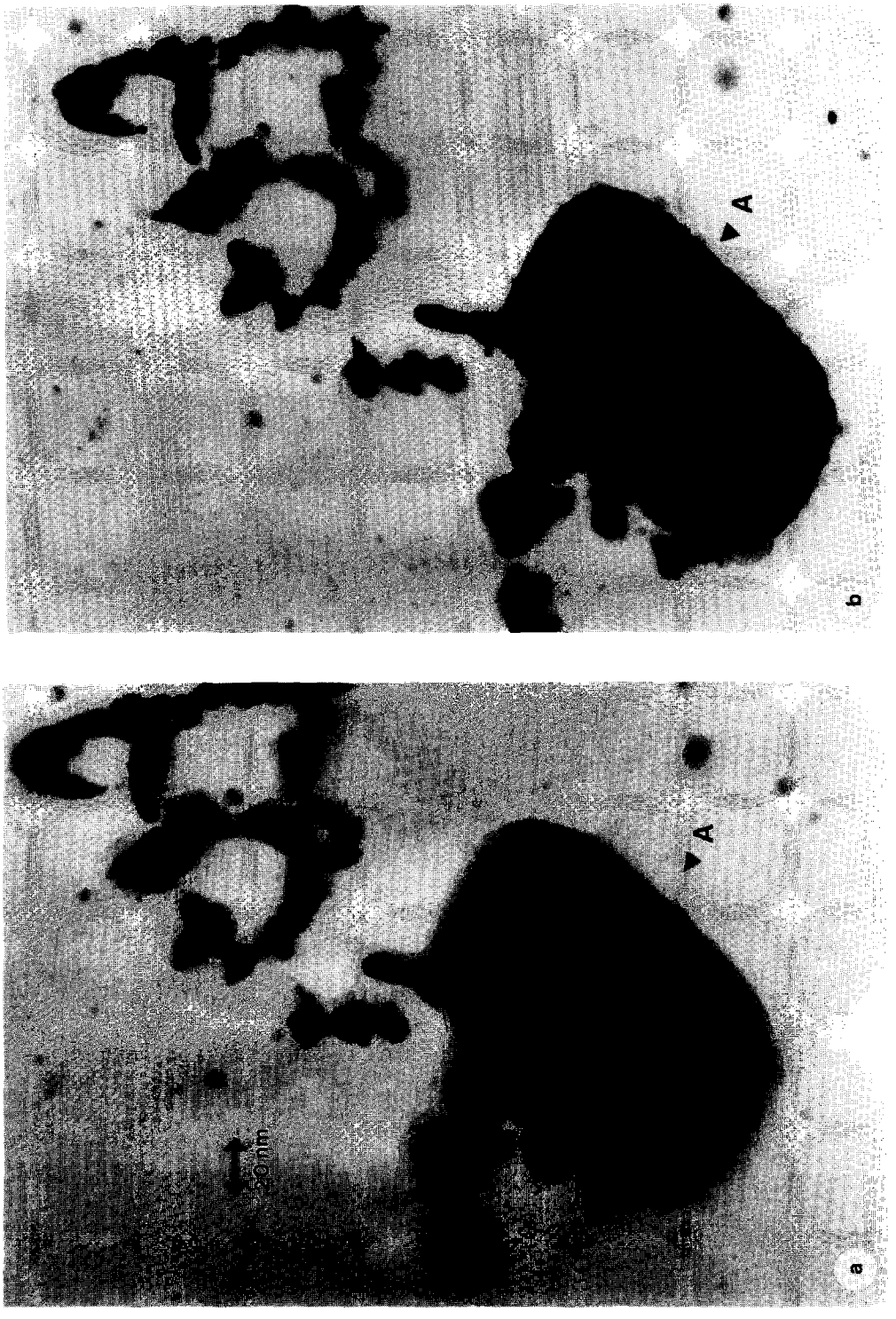

FIG. 5. Disintegration of overlayers upon exposure to the electron beam (a) immediately after exposure, (b) 4 min after.

ent in the microscope background pressure. However, this mechanism would have led to the growth of overlayers with electron beam exposure and not, as observed, to their disintegration (Fig. 5). Carbon contamination was purposely induced in several areas of the catalysts by prolonged exposure to the electron beam (20 min to 2 h) which did not lead to overlayers, but to an even discoloring of the entire region. Another mechanism possibly leading to overlayer formation would be growth from the silica substrate or from impurities in the precursor salt solutions. This mechanism can be discounted on the basis that overlayers were not observed after calcination of the Pt/SiO_2 model catalysts sample. Furthermore, overlayers were not produced by exposure to ambient conditions, since the Pt/SiO_2 sample remained virtually unchanged after 10 weeks of storage.

Once extraneous effects due to contamination are discounted, it remains to explain what is the mechanism of overlayer formation after the second calcination. It has been reported in the literature that two forms of WO_3 exist supported on silica (*19*). At low loadings, WO_3 exists as a highly dispersed amorphous film, whereas bulk WO_3 forms at high loadings. We speculate that these two forms are present in our planar model catalyst due to nonuniformities in tungsta loading occurring during catalyst preparation. The bulk form is clearly seen in Fig. 2a after the high-temperature calcination, whereas the highly dispersed form is not resolved in the micrographs at the resolution and magnification used. Upon deposition of Pt and subsequent low-temperature calcination, two mechanisms can result in overlayer formation: (i) the highly dispersed form can migrate onto the bulk form, or (ii) bulk WO_3 can spread to yield the disperse form which can land on top of Pt crystallites in close proximity. The driving force for the first mechanism is an Oswald ripening process, as suggested by the shrinking of the small crystallites marked by 2 and 2′ in Fig. 2. In the second mechanism the lower surface free energy of the silica–WO_3 interface, discussed below, would lead to the spreading process. The second mechanism is well known in the preparation of supported molybdena catalysts and has been shown to occur in recent TEM studies of molybdena model catalysts similar to the ones employed in this work (*28*). Either one of these mechanisms can explain overlayer formation after calcination, and our results do not permit us to differentiate among them.

In a recent study of model Fe/Al_2O_3 catalysts using a similar microscope (*21*), in which iron oxide overlayers were seen surrounding Fe containing crystallites, the presence of an iron oxide film over the alumina support was inferred from the difference in sharpness of substrate grain boundaries before and after treatments. Such differences in the texture of the SiO_2 grain boundaries can be seen between the reduction and calcination steps in Figs. 2b and 2c and 3b and 3c.

The mechanisms outlined above also explain why overlayer formation is not observed in all areas. According to the first mechanism, migration requires that Pt and the highly dispersed form of WO_3 be in close proximity. In the second mechanism spreading might require a particular epitaxial relation with the silica support and the proximity of Pt crystallites. Lacking either one of these conditions might prevent formation of overlayers sufficiently broad to be resolved with the microscope used in this work.

The disintegration of overlayers by exposure to the electron beam also suggests they consisted of tungsten oxides. Irradiation by an electron beam is known to reduce WO_3 (*22*), and during reduction, volatile suboxides are produced (*23*). Any such volatiles produced would then be transported away by the microscope's vacuum system.

A thermodynamic argument also favors the formation of WO_3 overlayers over Pt. The surface free energy (σ) of WO_3 has been reported as 100 ergs/cm^2 at 1473°C

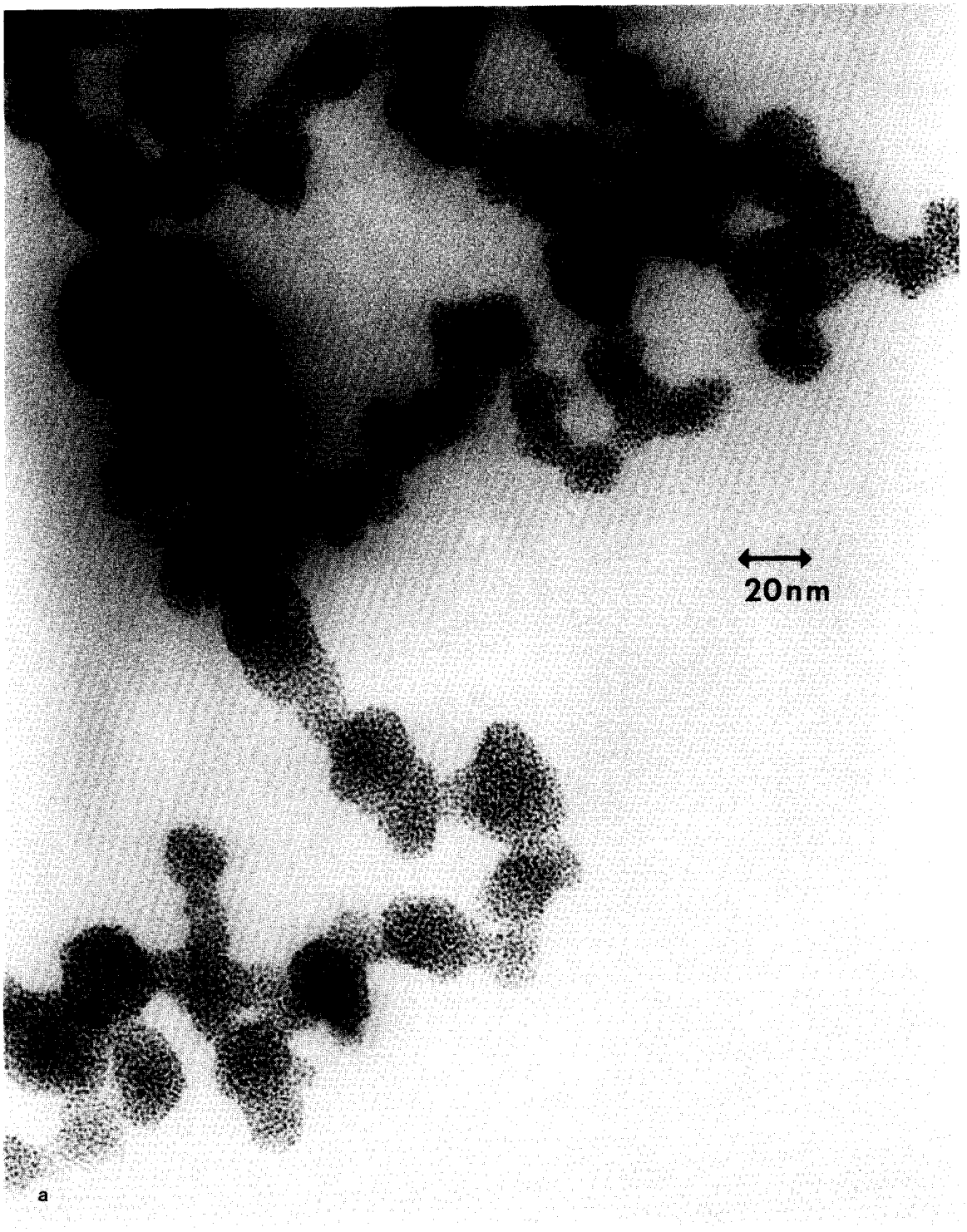

FIG. 6. $Pt–SiO_2$ single-component model catalyst (a) after impregnation and drying, (b) after low temperature calcination.

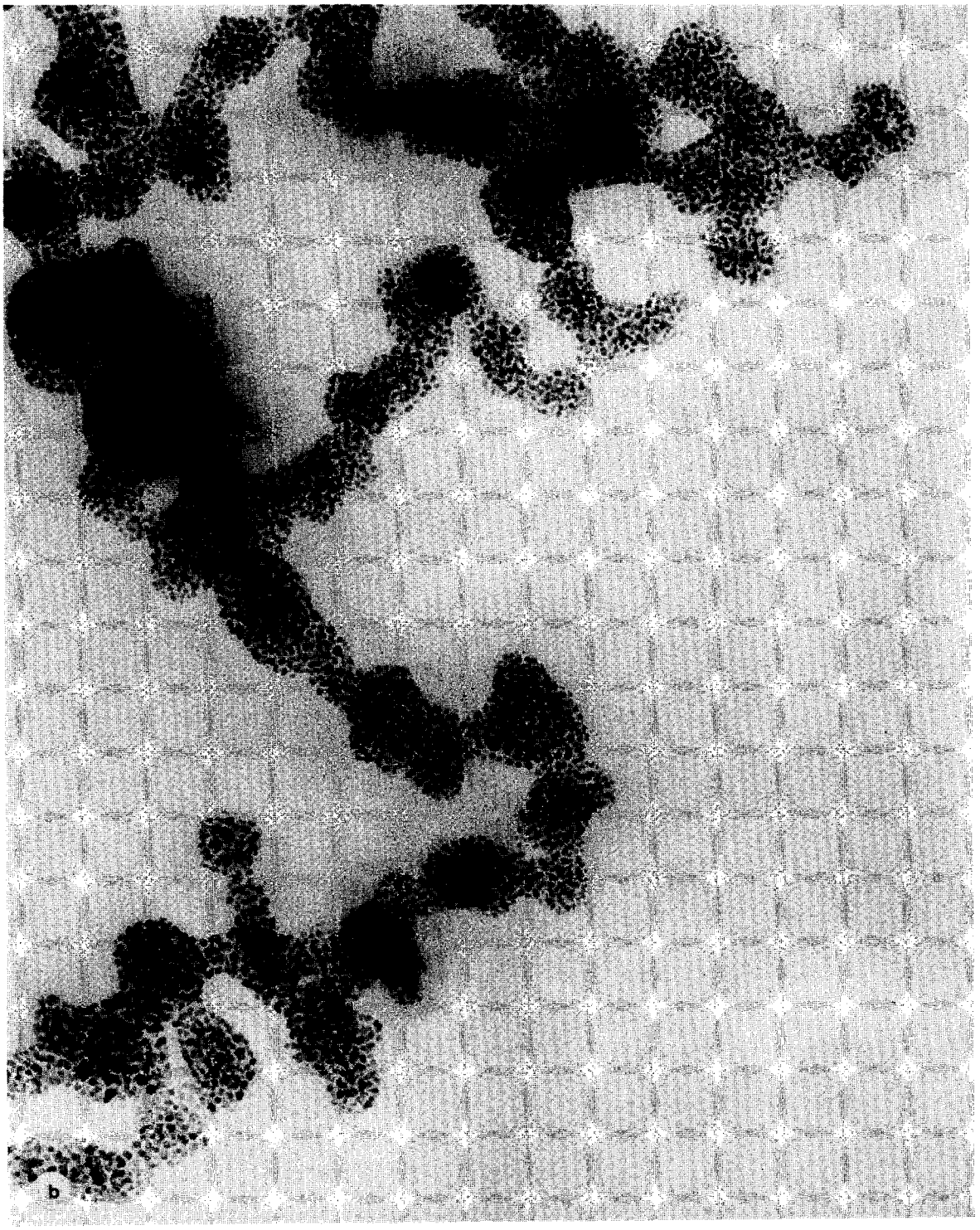

FIG. 6—*Continued.*

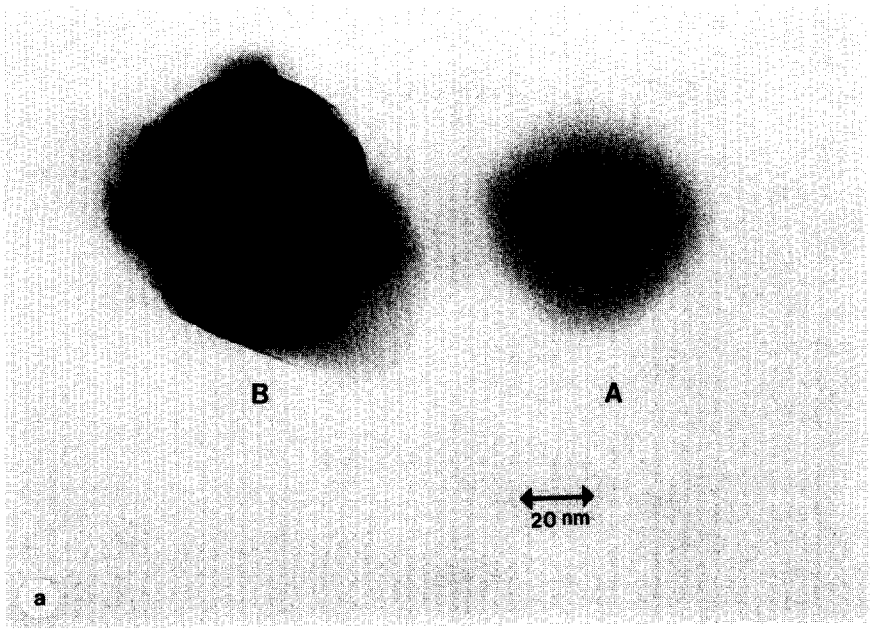

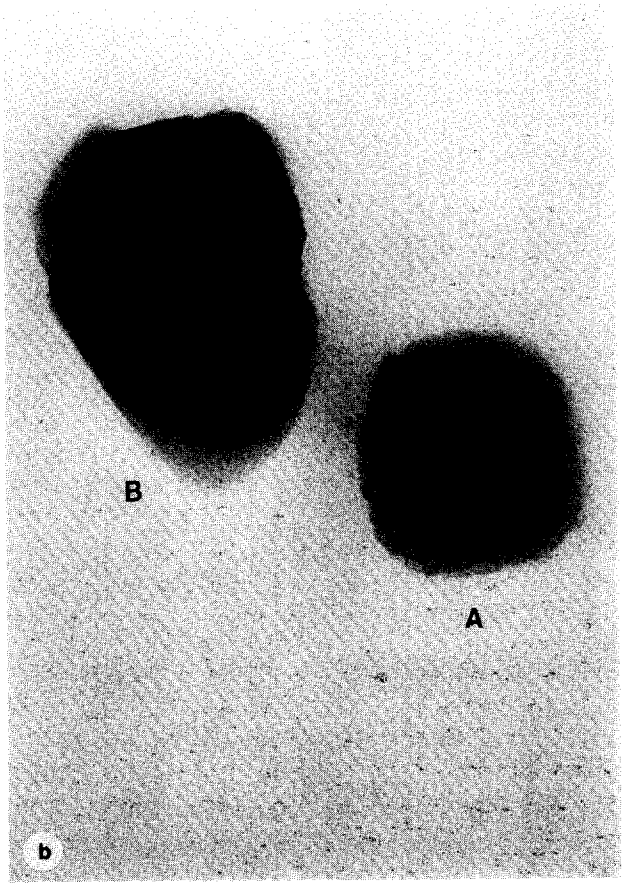

FIG. 7. WO_3–SiO_2 single-component model catalyst (a) after high-temperature calcination, (b) after low-temperature calcination.

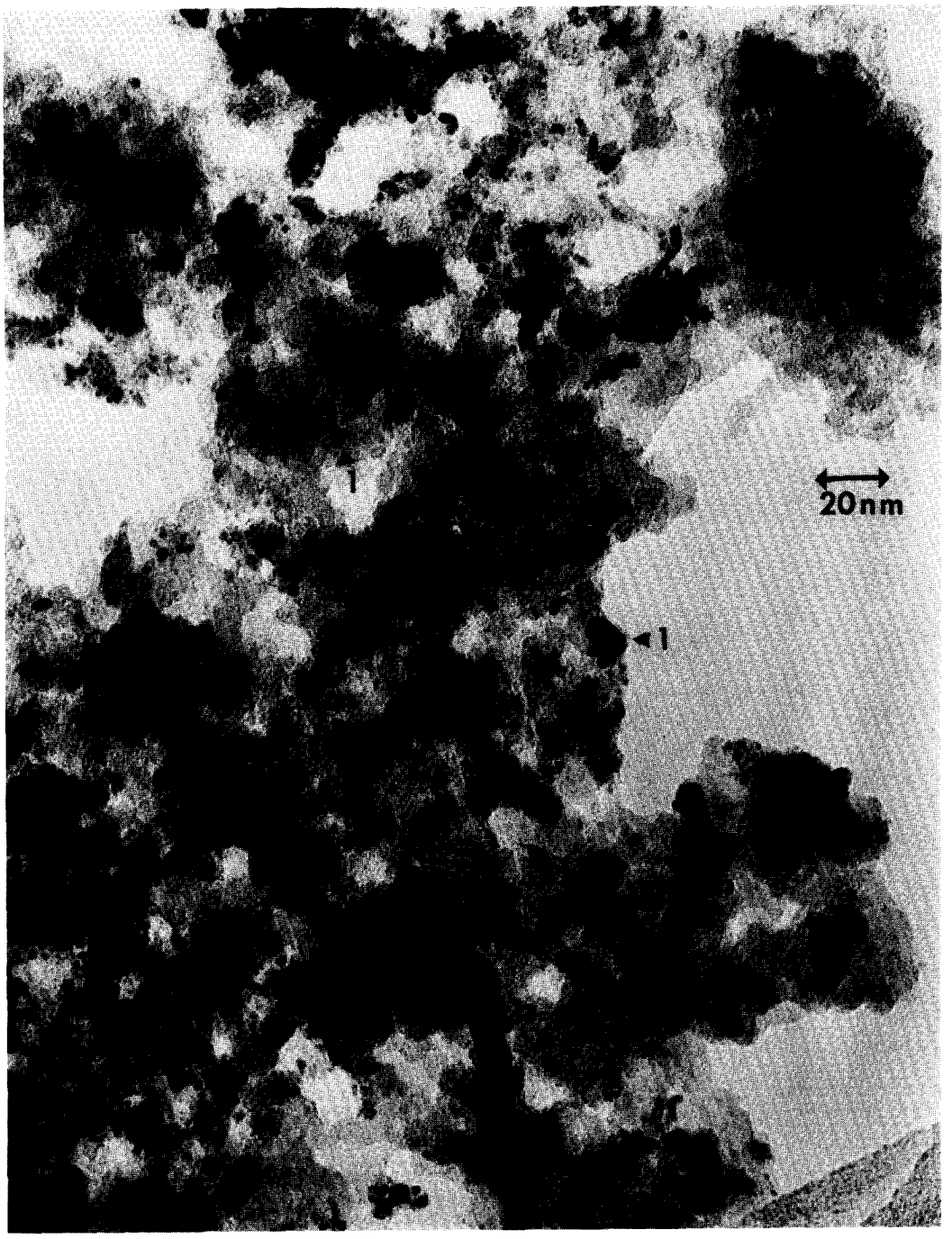

FIG. 8. Supported Pt/WO_3–SiO_2 catalyst after reduction.

(*24*). Correcting this to 298°C by using $d\sigma/dT = -0.1$ ergs/(cm^2 °C) (*25*) yields a value of 220 ergs/cm^2. In a recent comparison of SMSI versus non-SMSI supports (*25*) it has been shown that the surface tensions at 298°C, of various SMSI materials, are all below 560 ergs/cm^2 (the value for TiO_2) while all non-SMSI supports had higher values. The value for WO_3 estimated above falls well within the range of SMSI

materials. The surface tension for SiO_2 at 298°C is 605 ergs/cm^2; thus the spreading of WO_3 on SiO_2 would serve to lower the total surface free energy. Furthermore, the surface tension of Pt has been reported to be 2340 ergs/cm^2 at 1310°C (*26*). Therefore the driving force also exists for WO_3 to cover Pt, even preferentially to SiO_2.

The second calcination step thus appeared to play a major role in the formation of overlayers, in which highly dispersed surface complexes of WO_3 could form and migrate over the catalyst surface. The majority of decoration seems to have occurred during this step, as the morphology of the overlayers subsequently changed only slightly. Characterization of the real catalysts supports this conjecture; XPS Pt/Si ratios (*1*) were almost constant after calcination and after reduction. Decoration during the reduction step and not the calcination step would have caused an increase in the Pt/Si ratios. As a final note on the formation of overlayers during calcination, Fig. 7 (the WO_3/SiO_2 catalyst) reveals that WO_3 has itself some mobility. While in many ways the interaction between Pt and WO_3 is a synergistic one, the spreading of WO_3 does not appear to require the presence of Pt.

Reduction affected mainly the chemical states of the species present and only slightly their morphology. After reduction, a black coloration was observed even for the small amounts of WO_3 present on the microscope grid. This chromatic effect has been identified in previous XRD and XPS studies (*1*) of the real supported catalysts, as arising from mixed phases of HTB and WO_2. Electron diffraction patterns of the model catalysts did indicate the presence of HTB (Fig. 4c). If WO_2 formed in the model catalysts, the overlayers on Pt would be the preferred regions as they are the closest to the source of hydrogen spillover. The fact that overlayers on Pt were more stable than those on WO_3 also points to some interaction between Pt and WO_2 which stabilizes the Pt overlayers toward electron-stimulated reduction. Variation in the binding energy of Pt $4f_{7/2}$ observed in the real catalysts (*1*) also indicated an interaction between Pt and tungsta suboxides.

Overlayers were not observed in the real catalysts since, among other factors, resolution and contrast were never sufficient to distinguish overlayers from the support background. Nonetheless the lack of detection in the real catalyst does not prove that they do not form, but rather that conditions are rather difficult for its visualization via TEM (which is the reason why model catalysts were used in the first place). Overlayer formation was perhaps facilitated on the model sample due to the more facile diffusion on a relatively planar substrate than through a porous matrix. The less uniform and sometimes relatively high loading of the WO_3 on the model catalysts perhaps also increased migration of the mobile precursor and facilitated overlayer formation. Thus the size of the overlayers formed on the model catalysts is much exaggerated compared to the real catalyst. They are detectable in the model catalysts because conditions which promote overlayer growth are optimal.

Another difference between the real and the model catalysts is that no $PtCl_2$ was observed after the second calcination step by TEM. In a recent TEM investigation of the sintering and redispersion behavior of chlorided Pt catalysts (*27*), $PtCl_2$ was found to decompose into Pt crystallites very rapidly upon exposure to the electron beam. It is therefore possible that some of the small aggregated clumps of Pt did contain $PtCl_2$. Only a limited effort to identify $PtCl_2$ was made. Diffraction patterns of only a few regions were taken after the second calcination step because it was desired to minimize the exposure of the sample (and unstable overlayers) to the electron beam.

SUMMARY

The results obtained in this work indicate that a major step in determining the mor-

phology and texture of Pt crystallites was the impregnation and drying step. Calcination caused overlayer formation on the WO_3 and Pt phases, and caused slight sintering of the Pt crystallites. Reduction produced only slight changes in morphology and texture. After reduction, bulk WO_3 was transformed to HTB, and the overlayers on the Pt crystallites were believed to reduce to WO_2, as was shown for real $Pt/WO_3/SiO_2$ catalysts.

It should be reiterated that the trends observed on the model catalyst were not visualized in the real catalysts, but there was a good correlation between the model catalyst morphology to characterization studies performed on the real catalysts. Furthermore, exactly the same pretreatment steps were used for the real and model catalysts. Thus the model catalyst results are believed to represent an exaggerated version of events happening on a smaller scale in the more complex real catalyst. It should also be stressed that these results are representative for a model WO_3 and Pt containing catalyst, undergoing the specific sequence of pretreatments used in this work. Its extension to other systems for which similar models have been proposed, such as TiO_2, have yet to be proven.

ACKNOWLEDGMENTS

Some of the micrographs presented here were obtained with the generous assistance of Dr. Neil Long and the use of the microscopy facilities at the Department of Physics of Arizona State University.

REFERENCES

1. Regalbuto, J. R., Fleisch, T. H., and Wolf, E. E., *J. Catal.*, in press.
2. Tauster, S. J., *Amer. Chem. Soc. Symp. Ser.* **298,** 1 (1986).
3. Kelley, R. M., Short, D. R., and Swartzfager, D. G., *J. Mol. Catal.* **20,** 235 (1983).
4. Baker, R. T. K., Prestridge, E. B., and Garten, R. L., *J. Catal.* **56,** 390 (1978).
5. Baker, R. T. K., Prestridge, E. B., and Garten, R. L., *J. Catal.* **59,** 293 (1979).
6. Baker, R. T. K., Prestridge, E. B., and Murrell, M. M., *J. Catal.* **79,** 348 (1983).
7. Vis, J. C., van 't Black, H. F. J., Huizinga, T., van Grondelle, J., and Prins, R., *J. Catal.* **95,** 333 (1985).
8. Singh, A. K., Pande, N. K., and Bell, A. T., *J. Catal.* **94,** 422 (1985).
9. Dumesic, J. A., Stevenson, S. A., Sherwood, R. D., and Baker, R. T. K., *J. Catal.* **100,** 79 (1986).
10. Baker, R. T. K., France, J. A., Rouse, L., and Waite, R. J., *J. Cat.*, **41,** 22 (1976).
11. Baker, R. T. K., and Sherwood, D., *J. Catal.* **61,** 378 (1980).
12. Schmidt, L. D., Wang, T., and Vacquez, A., *Ultramic* **8,** 175 (1982).
13. Hicks, R. F., Yen, Q.-J., Bell, A. T., and Fleisch, T., *Appl. Surf. Sci.* **19,** 315 (1984).
14. Hicks, R. F., Yen, Q.-J., and Bell, A. T., *J. Catal.* **89,** 498 (1984).
15. Regalbuto, J. R., and Wolf, E. E., *J. Catal.*, in press.
16. Sermon, P. A., and Bond, G. C., *J. Chem. Soc. Faraday Trans. 1* **72,** 730 (1976).
17. Dickens, P. G., and Hurditch, R. J., *in* "The Chemistry of Extended Defects in Non-Metallic Solids (L. Eyring and M. O'Keefe, Eds.). North-Holland, Amsterdam, 1970.
18. Lyman, C. E., *J. Mol. Catal.* **20,** 357 (1983).
19. Biloen, P., and Pott, G. T., *J. Catal.* **30,** 169 (1973).
20. Thomas, R., van Oers, E. M., De Beer, V. H. J., and Moulijn, J. A., *J. Catal.* **84,** 275 (1983).
21. Ruckenstein, E., and Sushuma, I., *J. Catal.* **97,** 1 (1986).
22. Amelinckx, S., and Van Landuyt, J., *in* "The Chemistry of Extended Defects in Nonmetallic Solids" (Eyring, L., and O'Keefe, M., Eds.). North-Holland, Amsterdam, 1970.
23. Taskinen, P., Hytonen, P., and Tikkanen, M. H., *Scand. J. Met.* **6,** 228 (1977).
24. Overbury, S. H., Bertrand, P. A., and Somorjai, G. A., *Chem. Rev.* **75**(5), 547 (1975).
25. Ruckenstein, E., *ACS Symp. Serv.* **298,** 152 (1986).
26. Ruckenstein, E., and Chu, Y. F., *J. Catal.* **59,** 109 (1979).
27. Foger, K., and Jaeger, H., *J. Catal.* **92,** 64 (1985).
28. Regalbuto, J. R., personal communication.